Inorganic Chemistry

pubs.acs.org/IC Article

Redox-Controlled Reactivity at Boron: Parallels to Frustrated Lewis/Radical Pair Chemistry

3 Anthony Wong, Ijaxiang Chu, Guang Wu, Joshua Telser, Roman Dobrovetsky, and Gabriel Ménard*



Cite This: https://dx.doi.org/10.1021/acs.inorgchem.0c01464



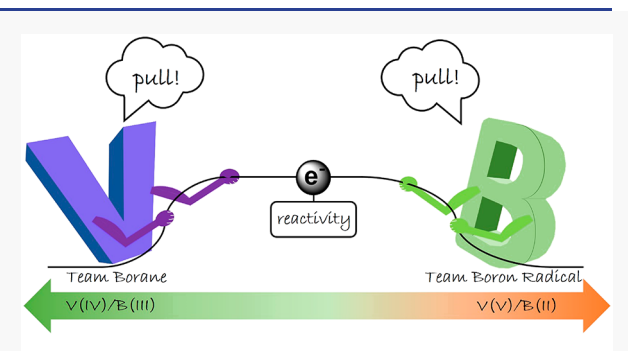
ACCESS

III Metrics & More

Article Recommendations

s Supporting Information

4 **ABSTRACT:** We report the synthesis of new Lewis-acidic boranes 5 tethered to redox-active vanadium centers, $(Ph_2N)_3V(\mu\text{-N})B(C_6F_5)_2$ 6 (1a) and $(N(CH_2CH_2N(C_6F_5))_3)V(\mu\text{-N})B(C_6F_5)_2$ (1b). Redox 7 control of the $V^{IV/V}$ couple resulted in switchable borane versus 8 "hidden" boron radical reactivity, mimicking frustrated Lewis versus 9 frustrated radical pair (FLP/FRP) chemistry, respectively. Whereas 10 heterolytic FLP-type addition reactions were observed with the V^V 11 complex (1b) in the presence of a bulky phosphine, homolytic peroxide, 12 or Sn-hydride, bond cleavage reactions were observed with the V^{IV} 13 complex, $[CoCp_2^*][(N(CH_2CH_2N(C_6F_5))_3)V(\mu\text{-N})B(C_6F_5)_2]$ (3b), 14 indicative of boron radical anion character. The extent of radical 15 character was probed by spectroscopic and computational means. 16 Together, these results demonstrate that control of the $V^{IV/V}$ oxidation 17 states allows these compounds to access reactivity observed in both FLP 18 and FRP chemistry.



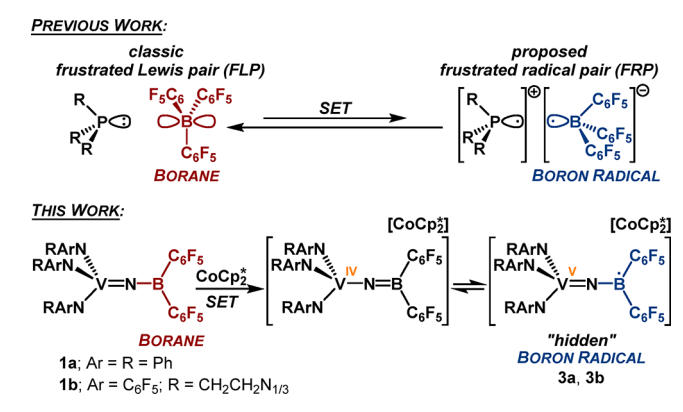
A radical "tug-of-war" between V and B enables bond activation mimicking frustrated Lewis or radical pair chemistry through V^{IV/V} redox control.

19 INTRODUCTION

20 The past two decades have seen a dramatic increase in 21 reported main-group-mediated bond activation chemistry. 1-5 22 Frustrated Lewis pair (FLP) chemistry has been a significant 23 contributor to this increase, stimulating intrigue spanning 24 multiple fields while unlocking new applications in main-group 25 chemistry. 6-8 Whereas FLPs can activate an ever-expanding 26 repertoire of small molecules (H₂, CO₂, N₂O, CO, etc.) and 27 bonds (C-H, alkenes, alkynes, etc.), the commonly accepted 28 mechanism features initial element-element bond polarization 29 within the pocket of an "encounter complex" generated by the 30 close interaction of the Lewis pair, followed by a two-electron, 31 concerted heterolytic bond activation step. 9-11 However, 32 recent work has uncovered a possible homolytic pathway 33 mediated by transient ionic phosphine/borane frustrated 34 radical pairs (FRPs) generated by single-electron transfer 35 (SET) (Scheme 1). 12-18 The existence of these FRPs was 36 supported by combined spectroscopic (i.e., EPR) and 37 reactivity studies, with the latter focusing on the unique 38 chemistry of the generated boron radical anion, such as 39 homolytic peroxide or Sn-hydride bond cleavage, similar to 40 related reports using isolated boron radical species. 19-23

Our group has been exploring new reactivity at main-group 42 centers by tethering these to redox-active metal centers, such 43 as V or Fe. $^{24-28}$ In a recent contribution, we uncovered how a 44 typically unreactive P^V =O bond tethered to a neighboring V^V 45 center in the complexes $(Ph_2N)_3V$ =N- $P(O)Ar_2$ $(Ar = Ph, 46 C_6F_5)$ can engage in H atom $(H\cdot)$ or silyl group $(Me_3Si\cdot)$ 47 transfer chemistry, resulting in the proposed protonation or

Scheme 1^a



"Classical FLP containing a bulky phosphine with a bulky borane and proposed FRP generated by SET containing a boron radical anion (top). This work highlights the switchable reactivity from a borane to a "hidden" boron radical anion by redox control (bottom).

Received: May 20, 2020



48 isolated silylation of the P^V =O bond, respectively, with the 49 concurrent reduction of V^V to V^{IV} . Similar reactivity was not 50 observed in related all-main-group model compounds (ex. 51 Ph_3PO), highlighting the cooperative role of the metal center 52 in enabling new main-group-centered reactivity. In this Article, 53 we targeted V-tethered Lewis-acidic B complexes (1a,b), 54 which, by control of the V redox state, exhibited either FLP 55 chemistry in the borane (V^V) state or reactivity analogous to 56 the B partner in FRPs when in the boron radical anion (V^{IV}) 57 state (Scheme 1). The borane engaged in heterolytic bond 58 activation chemistry, whereas the "hidden" boron radical anion 59 reacted homolytically. This complementary reactivity profile 60 draws significant parallels to the alternating reactivity found in 61 FLPs versus FRPs.

62 RESULTS AND DISCUSSION

63 The synthesis of our initial target complexes (1a,b) followed 64 an analogous approach to our previously reported $(Ph_2N)_3V$ =65 N-P(O)Ar₂ ("VNP") complexes²⁸ and involved salt meta-66 thesis between $ClB(C_6F_5)_2^{29}$ and the known precursor, 67 $(Ph_2N)_3V(\mu\text{-N})\text{Li}(THF)_3$, 30 or the new tren-based precursor, 68 $N(CH_2CH_2N(C_6F_5))_3V(\mu\text{-N})\text{Li}(THF)_3$, to yield complexes 69 1a and 1b, respectively (Scheme 1). The tren-based precursor 70 was prepared in three steps by initial acid—base metalation 11 using the known protonated ligand³¹ and $V(NTMS_2)_3$, 32 followed by V^V imine formation with TMSN₃ and desilylation 73 using iPrNHLi (see the Experimental Section). 30 Single 74 crystals suitable for X-ray diffraction (XRD) studies were 75 grown for both 1a and 1b. The solid-state structures for 1a 76 (Figure 1) and 1b (Figure S70) revealed expected trigonal

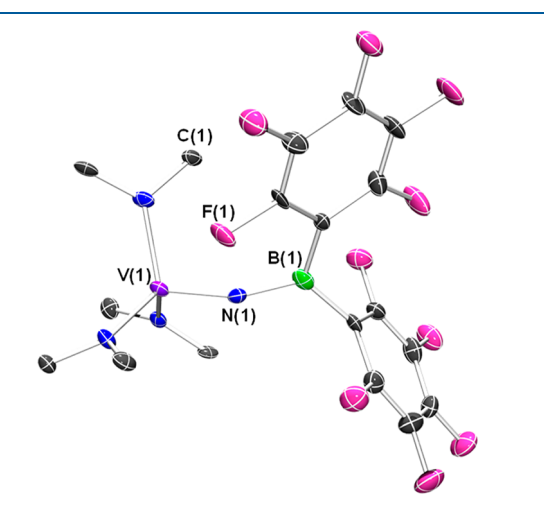


Figure 1. Solid-state molecular structure of 1a. C_6H_5 groups (except for ipso carbons) and all hydrogen atoms are omitted for clarity.

77 planar B centers with observed B-N (1.421(11) Å (1a); 78 1.428(6) Å (1b)) and neighboring V=N (1.670(6) Å (1a), 79 1.703(4) Å (1b)) bond lengths similar to previous reports. 880 The resulting V=N-B angles differed substantially from one 81 another (161.1(6)° (1a), 170.0(3)° (1b)). with both deviating 82 more from linearity than in the reported VNP case 83 (175.9(7)°). The analysis of the products by multinuclear 84 nuclear magnetic resonance (NMR) spectroscopy revealed 85 expected broad 11 B resonances (31.8 ppm (1a), 30.1 ppm 86 (1b)) consistent with three-coordinate B centers. 33,34 Whereas 87 the 51 V resonance for 1a (120 ppm) was similar to that of the 88 VNP analog (117 ppm), 28 the resonance for 1b (-79 ppm)

was significantly shifted, likely due to the higher coordination 89 number at V. 35 Whereas borane-substituted early metal imido 90 complexes are known, 36-42 to the best of our knowledge, these 91 represent the first examples incorporating boranes with 92 strongly electron-withdrawing substituents. 93

We observed that 1a was unstable and readily decomposed 94 within hours in solution at room temperature, as observed by 95 multinuclear NMR spectroscopy (Figures S50-S52). One of 96 the decomposition products, $Ph_2NB(C_6F_5)_2$, was identified 97 through independent synthesis, whereas the V-containing 98 decomposition product remains unknown (Figures S46- 99 S49). We attributed this decomposition pathway to the close 100 proximity of the Lewis-acidic B center to the labile Lewis-basic 101 Ph₂N⁻ groups. Dissolving 1a in coordinating solvents 102 (tetrahydrofuran (THF), MeCN) led to adduct formation 103 and slower decomposition, as observed by NMR spectroscopy 104 (Figures S62 and S63). The coordinating solvent molecules 105 could be readily removed in vacuo, indicating reduced Lewis 106 acidity at B in 1a compared with $B(C_6F_5)_3$, 43 the Lewis acid of 107 choice in FLP chemistry. 6-8 Not surprisingly, the decom- 108 position pathway observed in 1a was not observed in 1b due to 109 the chelating tren ligand.

We next investigated whether 1b could act as an effective 111 Lewis acid partner in FLP chemistry. Whereas combinations of 112 1b with bulky phosphines (PtBu₃, PMes₃, Mes = 2,4,6-113trimethylphenyl) led to no changes in the NMR spectra 114 compared with isolated Lewis partners—the hallmark of FLP 115 formation—no reaction with small molecules (H2, CO2) was 116 observed. Whereas the reduced Lewis acidity at B may be 117 partially responsible, we believe that the extreme steric 118 crowding at B due to the flanking tren aryl groups, as observed 119 in the space-filling depiction of the solid-state structure (Figure 120 S71), likely plays a bigger role. Therefore, we attempted to use 121 a more donating, "longer" para-benzoquinone molecule, 122 previously used in FLP chemistry. 12 Mixing equimolar 123 amounts of 1b, PMes₃, and tetrafluoro-1,4-benzoquinone in 124 dichloromethane (DCM) resulted in the immediate formation 125 of a new product (Figure 2a), as observed by NMR 126 f2 spectroscopy. Single crystals suitable for XRD studies were 127 obtained and confirmed the formation of compound 2-F4 128 (Figure 2b), featuring the FLP addition across the 129 benzoquinone moiety. We note that the analogous reaction 130 with unsubstituted benzoquinone to yield the product 2-H₄ 131 was also obtained, although it was only characterized 132 crystallographically (Figure S72). Lastly, we note that the 133 mechanism of activation here is unlikely to proceed through an 134 SET mechanism, sometimes proposed with PMes₃, ^{12,44} due to 135 the inability of 1b to oxidize PMes₃ to any appreciable extent 136 (vide infra).45

Whereas the B centers in **1a,b** are Lewis-acidic, we next 138 probed if boron radical character could be accessed by redox- 139 control. Because of the instability of **1a**, we only investigated 140 the electrochemical profile of **1b** by cyclic voltammetry (CV) 141 in DCM. A clean, reversible redox event at $E_{1/2} = -1.10$ V, 142 referenced to the ferrocene/ferrocenium (Fc/Fc⁺) redox 143 couple (Figure 3a), was observed and attributed to the V^{IV/V} 144 f3 redox couple. This reduced complex was chemically isolated by 145 treating **1b** with decamethylcobaltocene, CoCp* ($E_{1/2} = -1.94$ 146 V in DCM). We note here that **1a** could also be reduced 147 using this method, albeit in lower isolated yields due to its 148 instability. The reduced products, **3a** and **3b** (Scheme 1), were 149 slowly crystallized, and low-resolution solid-state structures 150 were obtained by XRD studies (Figures S73 and S74). We 151

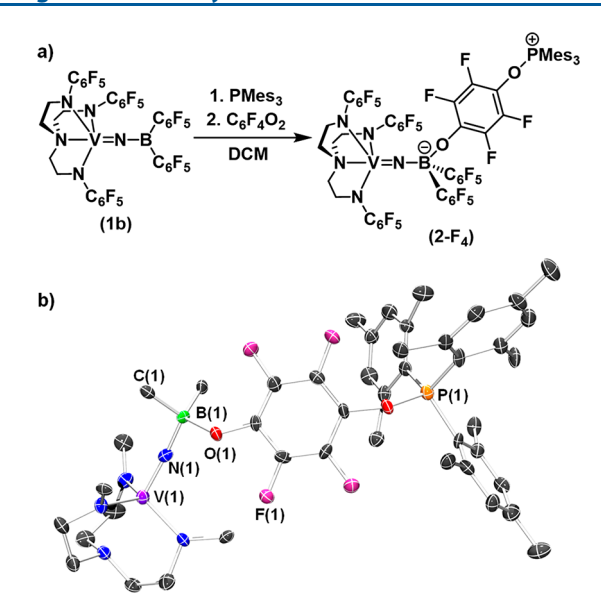


Figure 2. (a) FLP addition of $1b/PMes_3$ to tetrafluoro-1,4-benzoquinone to produce $2-F_4$. (b) Solid-state molecular structure of $2-F_4$. C_6F_5 groups (except for ipso carbons), hydrogen atoms, and cocrystallized solvent molecules are omitted for clarity.

152 note that a high-resolution structure was obtained by 153 generating a cobaltocene $(CoCp_2)$ analog of 3b, termed 3b' 154 (Figure S75). Both 3a and 3b' contained significantly 155 elongated V–N(B) bonds (1.885(8) Å (3a), 1.776(4) Å (3b')) and shortened B–N bonds (1.368(14) Å (3a), 1.354(7) ISF Å (3b')) relative to 1a,b (vide supra). The resulting V–N–B 158 angle in 3a was significantly more bent $(139.2(9)^\circ)$ relative to 159 1a $(161.1(6)^\circ)$, similar to the observed trend upon the 160 reduction of the VNP analog²⁸ and suggesting a simplified 161 single- and double-bonded structure (V-N=B) with the 162 reduction event mostly localized at V. In stark contrast, the V–163 N–B linkage in 3b' $(173.9(4)^\circ)$ changed only slightly relative 164 to 1b $(170.0(3)^\circ)$, which may suggest a more delocalized

V:-:N:-:B π framework enforced by the flanking tren aryl 165 groups.

Compounds 3a and 3b/3b' were further analyzed by X- 167 band EPR spectroscopy. The room-temperature spectrum of 168 3a revealed an expected isotropic eight-line hyperfine splitting 169 pattern due to the coupling of the d¹ electron to the ⁵¹V center 170 (I = 7/2) (Figure S64). Anisotropic spectra were observed at 171 100 K for all species (Figure 3b, Figures S65-S67) and were 172 similar to our reported VNP system. 28 The lack of resolved 173 hyperfine coupling to ¹¹B suggests little to no delocalization of ¹⁷⁴ the d¹ electron along the V-N-B framework. 47 However, 175 simulating the data in the absence of ¹¹B coupling led to ¹⁷⁶ sharper line widths and a poorer fit with the experimental data 177 (Figure S66), which may suggest some delocalization to B and 178 consequently N. The expected coupling to ¹¹B may simply be ¹⁷⁹ too weak to be observable by EPR spectroscopy. 48-50 180 Therefore, we turned to DFT studies to further probe this. 181 Calculations performed on the anion of 3b revealed some 182 degree of delocalization of the single electron to the B center 183 along the V:-N:-B π framework, suggesting the presence of a 184 "hidden" boron radical (Figure 3c). In particular, whereas the 185 majority of the spin density resided on V (82%), in agreement 186 with our EPR data, the spin density on B (13%) was found to 187 be non-negligible. 51 As previously noted, whereas several early 188 metal borylimido complexes have been prepared, 36-42 to the 189 best of our knowledge, their redox properties have not been 190 investigated as they have been here.

Similar to 1a, compound 3a was found to be very unstable in 192 noncoordinating solvents. Whereas we attributed the migration 193 of Ph_2N^- to B as being responsible for the decomposition of 194 1a, the decomposition of 3a was noticeably different. 195 Monitoring a solution of paramagnetic 3a in a mixture of 196 benzene- d_6 and bromobenzene- d_5 by multinuclear NMR 197 spectroscopy at room temperature revealed the appearance 198 of a main diamagnetic decomposition product (Figures S53–199 S55), with resonances in the ^{19}F (-127, -164, -167 ppm) 200 and ^{11}B (-2.0 ppm) spectra, consistent with the formation of a 201 four-coordinate boron center. 43 Interestingly, the ^{1}H NMR 202 spectrum revealed a major species having inequivalent 203

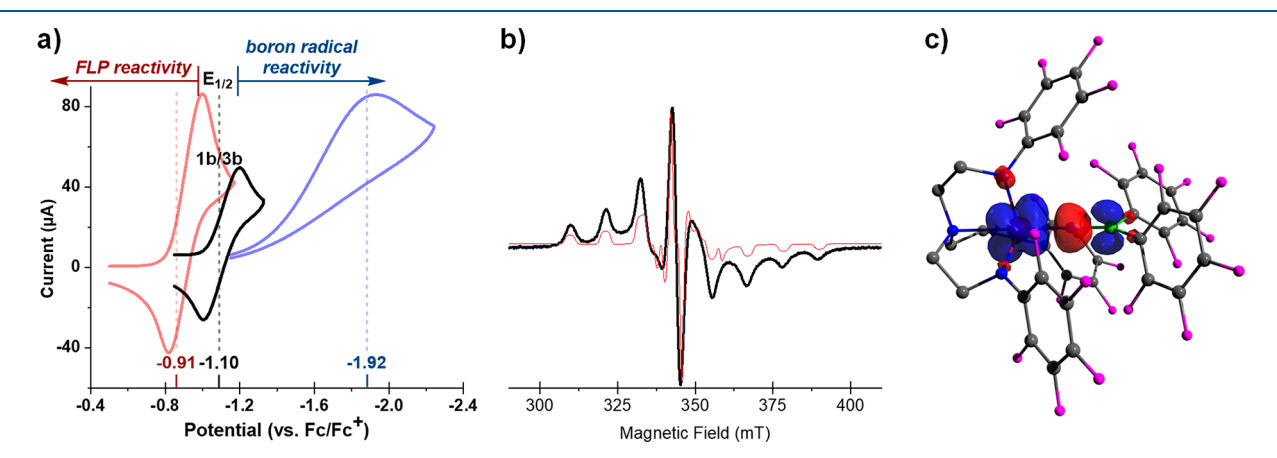


Figure 3. (a) Cyclic voltammograms (250 mV/s) of 1b (black) (3.0 mM), 2,4,6-tBu₃C₆H₂O· (red) (3.0 mM), and dibenzoyl peroxide (PhC(O)OOC(O)Ph) (blue) (3.0 mM) in DCM using 0.1 M [Bu₄N][PF₆] supporting electrolyte, a glassy carbon working electrode, a platinum wire counter electrode, and a Ag wire pseudoreference electrode and internally referenced to the Fc/Fc⁺ redox couple. Substrates possessing $E_{1/2} > -1.10$ V are susceptible to SET from 3b, leading to FLP reactivity (left), whereas those with $E_{1/2} < -1.10$ V are unlikely to be reduced and instead directly react with the "hidden" boron radical anion (right). (b) Anisotropic X-band EPR spectrum of 3b (black) with an overlaid simulation (red) at 100 K revealing a 51 V-centered reduction with possible electron delocalization along the V::N::B framework. (See the SI for simulation parameters.) (c) Spin-density map of 3b calculated by DFT and revealing a non-negligible contribution on B (13%), suggestive of "hidden" boron radical character.

204 resonances attributed to the $[\text{CoCp}_2^*]^+$ cation between 0.5 and 205 2.1 ppm (Figure S53). Upon scaling up the reaction, single 206 crystals suitable for XRD studies were grown, and the solid-207 state structure unequivocally revealed the formation of the 208 $[\text{CoCp}_2^*]^+$ C-H activated product, 4a (Figure 4). The bond 209 metrics along the V-N-B bonds in 4a are similar to those 210 found in 1a (Table S1) and are consistent with the observed 211 oxidation to a diamagnetic V^V center.

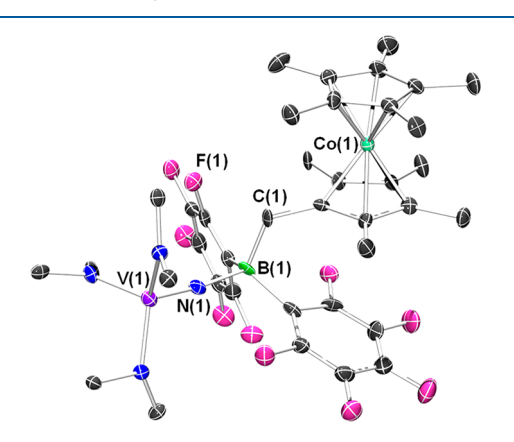


Figure 4. Solid-state molecular structure of **4a**. Phenyl C—H linkages, hydrogen atoms, and cocrystallized solvent molecules are omitted for clarity.

The methyl C-H bond activation of $[CoCp_2^*]^+$ in the 213 conversion of **3a** to **4a** involved the formal loss of H·, the fate 214 of which remains unknown. However, we observed that the 215 addition of the stable phenoxyl radical, 2,4,6- $tBu_3C_6H_2O$ -216 (**ArO·**), to **3a** resulted in the clean formation of **4a** and **ArOH**. 217 We also note that compound **3b** does not undergo this 218 spontaneous decomposition but does initiate the $[CoCp_2^*]^+$ 219 C-H activation in the presence of **ArO·**. Taken together, we 220 hypothesized that the C-H bond activation chemistry likely 221 proceeded through one of two mechanisms: (1) via a FRP-222 induced homolytic C-H cleavage mechanism involving the 223 **ArO·** and "hidden" boron radical anion (**3a,b**) (Scheme 2, left; 224 Figure 3c), reminiscent of previously proposed FRP⁴⁴ and 225 boron radical C-H reactivity, 21 or (2) via initial SET from the

Scheme 2^a

"Proposed FRP composed of the boron radicals 3a,b and ArOperforming C-H bond activation of $[CoCp_2^*]^+$ (left). Alternatively,
SET from 3a,b to ArO- would generate an FLP composed of 1a,b and ArO-, which could deprotonate the acidic methyl C-H bond in $[CoCp_2^*]^+$, generating the products 4a,b (right).

anion of 3a,b to ArO^{\bullet} to generate the FLP composed of ArO^{-} 226 and 1a,b (Scheme 2, right). Subsequent deprotonation at one 227 of the acidic methyl C-H bonds in $[CoCp_2^*]^+$ would result in 228 the formation of 4a,b. $^{52-54}$ A similar SET from a related borole 229 radical to TEMPO, followed by C-H deprotonation at 230 $[CoCp_2^*]^+$, was recently reported. 231

To distinguish between these possible mechanisms, a simple 232 comparison of the V^{IV/V} redox couple in 1/3 relative to the 233 $ArO^{\bullet/-}$ couple should reveal whether SET is favored. The CV 234 of $ArO^{\bullet/-}$ couple at $E_{1/2}=-0.91$ V vs Fc/Fc⁺ (Figure 3a). 236 Whereas the $E_{1/2}$ value of 1a/3a could not be obtained due to 237 the aforementioned instability of these complexes, the 1b/3b 238 couple at $E_{1/2}=-1.10$ V vs Fc/Fc⁺ (*vide supra*) does support a 239 favorable ($\Delta G=-19$ kJ/mol) SET event (Figure 3a). Thus 240 mechanistically, it is likely that the chemistry proceeded via an 241 FLP-type mechanism involving an initial SET from 3b to ArO• 242 to generate the $1b/ArO^-$ FLP, which initiated the observed 243 C–H functionalization.

Whereas the combination of 3a,b with ArO· likely generated 245 an intermediate FLP for C-H activation of [CoCp**]+, our 246 DFT studies nonetheless indicated that radical character at 247 boron should also be accessible (Figure 3c). As previously 248 noted, boron radicals are invoked in FRP chemistry and are 249 typically probed by homolytic bond cleavage reactions at 250 peroxides or Sn-hydrides. 19-23 To discount possible initial 251 SET to any of these reagents, we first collected the CV data of 252 both dibenzoyl peroxide (PhC(O)OOC(O)Ph) and Ph₃SnH. 253 The CV data of (PhC(O)OOC(O)Ph) collected in DCM 254 revealed an irreversible reduction event at $E_{\text{peak}}^{\text{red}} = -1.92 \text{ V}$ 255 (Figure 3a). Similarly, an irreversible reduction event was 256 observed for Ph₃SnH near the electrochemical window of 257 acetonitrile ($E_{\text{peak}}^{\text{red}} = -2.74 \text{ V}$, Figure S81). Thus any SET event 258 from 3b to either of these reagents should be highly 259 unfavorable ($\Delta G > 85 \text{ kJ/mol}$). Exposing either 3b or 3b' 260 (both paramagnetic) to a half-equivalent of PhC(O)OOC- 261 (O)Ph in DCM led to the clean emergence of new, 262 diamagnetic, analogous products, as observed by multinuclear 263 NMR spectroscopy. In particular, a sharp resonance in the ¹¹B ₂₆₄ NMR (-4.2 ppm), with corresponding meta/para-shifted 265 resonances in the ¹⁹F NMR spectra (Figures S41-S45), 266 emerged and is consistent with four-coordinate boron 267 centers. 43 A significantly shifted 51V NMR resonance (-311 268 ppm) also emerged from this reaction. Whereas suitable single 269 crystals for XRD studies were not obtained from the 3b 270 reaction, they were obtained from the 3b' reaction, albeit in 271 low resolution, and the solid-state structure confirmed the 272 formation of a new carboxylate B–O product (5b') generated 273 through the homolytic peroxide cleavage expected from boron 274 radical reactivity (Figure 5). $^{19-23}$ We note that the reaction 275 fs with 3a produced the analogous carboxylate product, 5a 276 (Figure S77).

Lastly, we explored the reactivity of 3b/3b' with Ph₃SnH. 278 While again the emergence of diamagnetic products was 279 observed by NMR spectroscopy, including a doublet resonance 280 in the ¹¹B NMR spectrum that collapsed to a singlet in the 281 ¹¹B{¹H} spectrum, indicating a B–H bond, we were unable to 282 obtain a clean product in this case (Figures S57–S61). 283 However, the analysis of the ¹¹⁹Sn NMR spectrum revealed the 284 formation of a single new product with a chemical shift at 285 –142.4 ppm (Figure S60), similar to those reported for 286 Ph₃SnSnPh₃ in various solvents. ¹² Upon working up the crude 287 reaction mixture, this product was isolated and unambiguously 288

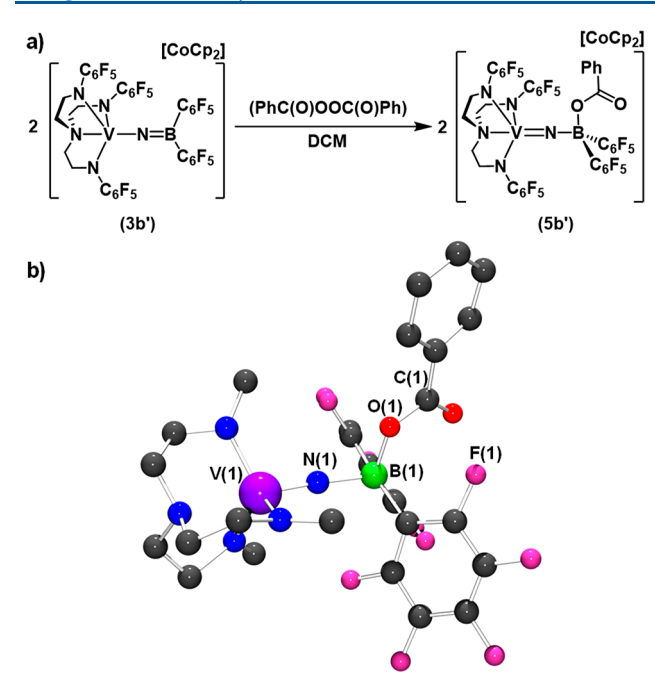


Figure 5. (a) Reaction of 3b' with PhC(O)OOC(O)Ph led to homolytic peroxide cleavage and B–O carboxylate bond formation (5b'), indicative of boron radical reactivity. (b) Low-resolution isotropic solid-state molecular structure of 5b'. C_6F_5 groups on tren (except for ipso carbons), $[CoCp_2]^+$, hydrogen atoms, and cocrystallized solvent molecules are omitted for clarity.

289 identified by XRD studies because its unit-cell parameters 290 matched the reported values. ⁵⁵ The formation of this Sn–Sn 291 product is strongly indicative of boron radical reactivity and 292 homolytic bond cleavage, analogous to reported FRP 293 reactivity. ^{19–23}

O4 CONCLUSIONS

295 In summary, we have outlined the synthesis of new Lewis-296 acidic boranes tethered to redox-active vanadium centers. 297 Redox control of the $V^{IV/V}$ pair allowed for controlled borane 298 or boron radical anion reactivity mimicking FLP or FRP 299 reactivity, respectively. We are further investigating the 300 potential use of such main-group/metal platforms for new 301 cooperative small-molecule or bond-activation chemistry.

302 **EXPERIMENTAL SECTION**

General Considerations. All manipulations were performed 304 under an atmosphere of dry, oxygen-free N2 or Ar through standard 305 Schlenk or glovebox techniques (MBraun UNIlab Pro SP Eco 306 equipped with a -38 °C freezer). Pentane, diethyl ether, benzene, 307 toluene, THF, and DCM were dried using an Mbraun solvent purification system. 2,2,4-Trimethylpentane (iso-octane), hexame-309 thyldisiloxane (HMDSO), acetonitrile, acetonitrile- d_3 , benzene- d_{60} 310 chloroform-d, dichloromethane- d_2 , and tetrahydrofuran- d_8 were 311 purchased from Aldrich or Cambridge Isotope Laboratories, degassed 312 by freeze-pump-thaw, and stored on activated 4 Å molecular sieves 313 prior to use. Ph₂NH, "BuLi (1.6 M in hexanes), VCl₃(THF)₃, 314 Me₃SiN₃, ⁱPr₂NH, and (PhC(O)OOC(O)Ph) were purchased from 315 Aldrich, Strem, or other commercial vendors and used as received. 316 $Co(C_5Me_5)_2$ and $Co(C_5H_5)_2$ were purchased from Aldrich and 317 sublimed prior to use. $(C_6F_5)_2BCl_1^{29}$ $(Ph_2N)_3V(\mu-N)Li(THF)_3^{30}$ 318 2,4,6- $^tBu_3C_6H_2O\cdot_5^{56}$ $N(CH_2CH_2NH(C_6F_5))_3^{31}$ $V(NTMS_2)_3^{32}$ and 319 PrNHLi³⁰ were prepared according to literature procedure. Elemental 320 analyses (C, N, H) were performed at the University of California, 321 Berkeley using a PerkinElmer 2400 Series II combustion analyzer.

Spectroscopic Analyses. NMR spectra were obtained on a 322 Varian Unity Inova 600 MHz, Varian Unity Inova 500 MHz, or 323 Agilent Technologies 400 MHz spectrometer and referenced to the 324 residual solvent of acetonitrile- d_3 (1.94 ppm), benzene- d_6 (7.16 ppm), 325 D₂O (4.79 ppm), dichloromethane- d_2 (5.32 ppm), methanol- d_4 (3.31 326 ppm), or tetrahydrofuran- d_8 (1.73 ppm) or externally (¹¹B: BF₃·Et₂O; 327 ¹⁹F: CFCl₃; ⁵¹V: VOCl₃; ³¹P: 85% H₃PO₄; ¹¹⁹Sn: Me₄Sn; ⁷Li: 9.7 M 328 LiCl in D₂O). Chemical shifts (δ) are recorded in ppm, and the 329 coupling constants are in hertz. X-band EPR spectra were collected on 330 a Bruker EMX EPR spectrometer equipped with an Oxford ESR 900 331 liquid-helium cryostat. A modulation frequency of 100 kHz was used 332 for all EPR spectra, and the data were plotted using Origin. EPR 333 simulations used the program QPOWA by Belford and coworkers, as 334 modified by J. Telser.⁵⁷

X-ray Crystallography. Data were collected on a Bruker KAPPA 336 APEX II diffractometer equipped with an APEX II charge-coupled 337 device (CCD) detector using a TRIUMPH monochromator with a 338 Mo K α X-ray source (α = 0.71073 Å). The crystals were mounted on 339 a cryoloop with Paratone-N oil, and all data were collected at 100(2) 340 K using an Oxford nitrogen gas cryostream system. A hemisphere of 341 data was collected using ω scans with 0.5° frame widths. Data 342 collection and cell parameter determination were conducted using the 343 SMART program. Integration of the data frames and final cell 344 parameter refinement were performed using SAINT software. 345 Absorption correction of the data was carried out using SADABS. 346 Structure determination was done using direct or Patterson methods 347 and difference Fourier techniques. All hydrogen atom positions were 348 idealized and rode on the atom of attachment. The structure solution, 349 refinement, graphics, and the creation of publication materials were 350 performed using SHELXTL or OLEX.2 All POV-Ray depictions of 351 the solid-state molecular structures are shown at the 50% probability 352 ellipsoid level unless otherwise noted.

Électrochemical Analyses. CV was performed on a CH 354 Instruments 630E electrochemical analysis potentiostat, equipped 355 with a 3 mm diameter glassy carbon working electrode, a Ag wire 356 pseudoreference electrode, and a Pt counter electrode with $[Bu_4N]$ - 357 $[PF_6]$ (0.1 M) supporting electrolyte solution in CH_2Cl_2 or CH_3CN . 358 The glassy carbon working electrode was cleaned prior to each 359 experiment by polishing with 1, 0.3, and 0.05 mm alumina (CH 360 Instruments) in descending order, followed by sonication in distilled 361 water for 2 min. All voltammograms were referenced to the Fc/Fc^+ 362 redox couple.

Density Functional Theory Calculations. DFT calculations 364 were performed using ORCA 4. The geometry optimization of the 365 anion of **3b** was carried out using the UKS TPSSO method with the 366 def2-TZVP basis set 59-61 and with the relativistic effect, which was 367 accounted for by the zero-order regular approximation (ZORA), 62-64 368 implemented in the ORCA software. The electric and magnetic 369 hyperfine structure was calculated for B and V centers only. 370

Synthesis of $(Ph_2N)_3V(\mu-N)B(C_6F_5)_2$ (1a). To a cold $(-35 \, ^{\circ}C)$ 371 solid mixture of ClB(C_6F_5)₂ (0.190 g, 0.5 mmol) and $(Ph_2N)_3V(\mu$ - 372 N)Li(THF)₃ (0.414 g, 0.5 mmol) was added cold ether (10 mL, -35 373 $^{\circ}$ C). The reaction solution stood at -35 $^{\circ}$ C for 2 days with 374 intermittent stirring for 1 min every 12 h. The mixture was filtered; 375 then, the solvent was removed in vacuo. The residue was washed with 376 cold pentane (4 × 5 mL), and the solid was dried in vacuo for 20 min 377 to afford a dark-brown solid (0.310 g, 0.34 mmol, 68% yield). Single 378 crystals suitable for XRD studies were obtained by cooling a 379 concentrated toluene/pentane solution of 1a to -35 °C and standing 380 overnight. 1 H NMR (400 MHz, $C_{6}D_{6}$, 25 $^{\circ}$ C): δ = 6.91–6.85 (m, 381 24H; ArH), 6.71 (m, 6H; ArH). A small amount of THF and ether 382 (\sim 0.5 equiv total) in the product could not be removed in vacuo, 383 which may due to the Lewis acidity of 1a. 13C NMR (100 MHz, 384 C_6D_6 , 25 °C): δ = 154.4, 128.9, 125.5, 123.2 (*Ph*₂N). The signal-to- 385 noise ratio was too low to properly identify any C_6F_5 ¹³C resonances. 386 ⁵¹V NMR (105 MHz, C_6D_6 , 25 °C): $\delta = 119.6$ (br). ¹³B NMR (128 ₃₈₇ MHz, C_6D_6 , 25 °C): $\delta = 31.8$ (br). ¹⁹F NMR (376 MHz, C_6D_6 , 25 388 °C): $\delta = -131.0$ (m, 4F; o-C₆F₅), -151.7 (t, J = 18.8 Hz, 2F; p-C₆F₅), 389 -162.1 (m, 4F; m-C₆F₅). Elemental analysis (%) calc. for 390 $C_{48}H_{30}BF_{10}N_4V$ (1a) (914.5315 g·mol⁻¹): C, 63.04; H, 3.31; N, 391

392 6.13. Found: C, 60.14; H, 3.30; N, 6.06. Attempts to obtain 393 satisfactory elemental analysis consistently resulted in reduced carbon 394 percentages, likely due to incomplete combustion.⁶⁵

Synthesis of $(N(CH_2CH_2N(C_6F_5))_3)V(\mu-N)B(C_6F_5)_2$ (1b). Part 1: 396 Synthesis of ((tren)VNTMS). To a solution of N(CH2CH2NH- $(C_6F_5)_3$ (0.545 g, 0.846 mmol) in THF (3 mL) was added 398 $V(NTMS_2)_3$ (0.450 g, 0.846 mmol) in THF (5 mL). The purple 399 mixture was sealed in a heavy-walled reaction flask and heated to 70 400 °C for 3 h until a dark-green solution formed. Under a nitrogen 401 atmosphere, TMS-N₃ (1.1 equiv) was added, and the resulting 402 mixture was resealed and stirred for 5 h at 70 °C to yield a yellow-403 orange solution. The volatiles were removed in vacuo and washed 404 with pentane until the filtrate became nearly colorless. The filter-cake 405 was then washed with ether $(3 \times 1 \text{ mL})$ to give a bright-yellow 406 powder (0.659 g, 0.705 mmol, 83.3% yield). Bright-yellow single 407 crystals suitable for XRD studies were grown by vapor diffusion of 408 HMDSO into a saturated ether solution of the product. NMR data: ¹H NMR (400 MHz, C_6D_6 , 25 °C): $\delta = 3.30$ (t, $^3J_{HH} = 8.0$ Hz, 6H; 410 CH₂), 2.13 (t, ${}^{3}J_{HH}$ = 8.0 Hz, 6H; CH₂), -0.77 (s, 9H; CH₃). ${}^{13}C$ 411 NMR (100 MHz, C_6D_6 , 25 °C): $\delta = 57.8$ (CH₂), 53.3 (CH₂), -1.8 412 (CH₃). The signal-to-noise ratio was too low to properly identify any ¹³C resonances. ⁵¹V NMR (105 MHz, C_6D_6 , 25 °C): $\delta = -259.3$ 414 (br). ¹⁹F NMR (376 MHz, C₆D₆, 25 °C): $\delta = -149.2$ (d, J = 18.5 Hz, 415 6F; o-C₆F₅), -165.6 (m, 6F; m-C₆F₅), -166.1 (t, J = 21.5 Hz, 3F; p-416 C_6F_5). Elemental analysis (%) calc. for $C_{27}H_{21}F_{15}N_5SiV$ (779.5025 g· 417 mol⁻¹): C, 41.60; H, 2.72; N, 8.98. Found: C, 41.92; H, 2.69; N, 8.92. Part 2: Synthesis of ((tren)VNLi(THF)₃). To a cooled, stirring 419 solution of ((tren)VNTMS) (1.0 g, 1.28 mmol) in THF (4 mL) was 420 added PrNHLi (0.117 g, 1.79 mmol) as a suspension in pentane (3 421 mL) to induce an immediate darkening of the solution to yellow-422 green. The reaction was monitored by ¹⁹F NMR, and (if needed) 423 additional aliquots of PrNHLi reagent were added to ensure the 424 complete consumption of the starting material. The reaction was 425 stirred for 30 min before the volatiles were removed in vacuo. The 426 residue was washed with pentane (10 \times 2 mL) to give a dark 427 microcrystalline powder (0.850 g, 0.912 mmol, 71.3% yield). Single 428 crystals suitable for XRD studies were grown by the slow vapor 429 diffusion of pentane into a saturated solution of the product in THF. 430 NMR data: ¹H NMR (400 MHz, C_6D_6 , 25 °C): $\delta = 3.49$ (t, $^3J_{HH} =$ 431 8.0 Hz, 6H; tren CH_2), 2.99 (t, ${}^3J_{HH}$ = 8.0 Hz, 12H; THF CH_2), 2.17 432 (t, 6H; ${}^{3}J_{HH}$ = 8.0 Hz, 6H; tren CH_{2}), 1.32 (m, 12H; THF CH_{2}). ${}^{13}C$ 433 NMR (100 MHz, C_6D_6 , 25 °C): $\delta = 67.6$ (THF CH_2), 55.7 (tren 434 CH₂), 53.0 (tren CH₂), 25.4 (THF CH₂). The signal-to-noise ratio 435 was too low to properly identify any C₆F₅ ¹³C resonances. ⁵¹V NMR 436 (105 MHz, C_6D_6 , 25 °C): $\delta = -143.1$ (br). ¹⁹F NMR (376 MHz, 437 C₆D₆, 25 °C): $\delta = -149.9$ (d, J = 22.5 Hz, 6F; o-C₆F₅), -168.7 (t, J =438 21.1 Hz 6F; m-C₆F₅), -173.7 (t, J = 22.3 Hz, 6F; p-C₆F₅). Elemental 439 analysis (%) calc. for $C_{36}H_{36}F_{15}LiN_5O_3V$ (929.5735 g·mol⁻¹): C, 440 46.52; H, 3.90; N, 7.53. Found: C, 46.25; H, 3.98; N, 7.57.

Part 3: Synthesis of 1b. To a stirring solution of ((tren)VNLi-442 (THF)₃) (1.0 g, 1.076 mmol) in benzene was added $(C_6F_5)_2BCl$ (0.409 g, 1.076 mmol) in ether/benzene to give a dark-green solution 444 that was stirred for 2 h. The volatiles were removed in vacuo, and the 445 green oily residue was dissolved in DCM and filtered through a Celite 446 plug to remove LiCl. The dark-green residue was minimally dissolved 447 in benzene and then treated with acetonitrile (0.1 mL) to give a 448 yellow precipitate that was collected and washed with pentane (10 × 449 1 mL) and ether (5 \times 1 mL). Upon dissolution into a 1:1 benzene/ 450 THF mixture and the removal of all volatiles, an analytically pure dark-green powder was isolated (0.755 g, 0.719 mmol, 66.8% yield). 452 Single crystals suitable for XRD studies were obtained by slow vapor 453 diffusion of HMDSO into a saturated solution of the product in ether. 454 NMR data: ¹H NMR (400 MHz, C_6D_6 , 25 °C): $\delta = 3.30$ (t, ${}^3J_{HH} =$ 455 5.4 Hz, 6H; CH_2), 2.35 (t, ${}^{3}J_{HH}$ = 5.4 Hz, 6H; CH_2). ${}^{13}C$ NMR (100 456 MHz, C_6D_6 , 25 °C): $\delta = 60.6$ (CH₂), 53.1 (CH₂). The signal-to-noise 457 ratio was too low to properly identify any C₆F₅ ¹³C resonances. ⁵¹V 458 NMR (105 MHz, C_6D_6 , 25 °C): $\delta = -78.9$ (br). ¹³B NMR (128 459 MHz, C_6D_6 , 25 °C): δ = 30.1 (br). ¹⁹F NMR (376 MHz, C_6D_6 , 25 460 °C): $\delta = -133.1$ (br, 4F; B o-C₆F₅), -148.4 (br, 6F; tren o-C₆F₅), 461 -149.5 (br, 2F; B p-C₆F₅), -161.4 (br, 4F; B m-C₆F₅), -162.9 (br,

3F; tren p-C₆F₅), -164.9 (br, 6F; tren o-C₆F₅). Elemental analysis 462 (%) calc. for C₃₆H₁₂BF₂₅N₅V (1051.2386 g·mol⁻¹): C, 41.13; H, 1.15; 463 N, 6.66. Found: C, 41.27; H, 1.38; N, 6.67.

Synthesis of 2-F₄. To a stirring solution of **1b** (0.010 g, 0.0095 465 mmol) and PMes₃ (0.00369 g, 0.0095 mmol) in DCM (3 mL) was 466 added tetrafluoro-1,4-benzoquinone (0.00171 g, 0.0095 mmol) in 467 DCM (1 mL) to give an orange solution within minutes. The reaction 468 was stirred for 10 min before the volatiles were removed in vacuo. 469 The residue was washed with pentane $(3 \times 1 \text{ mL})$ and ether (1 mL) 470 to give a yellow powder (0.011 g, 0.0068 mmol, 71.4% yield). Single 471 crystals suitable for XRD studies were grown by the slow vapor 472 diffusion of pentane into a saturated solution of 2-F₄ in DCM. NMR 473 data: ¹H NMR (400 MHz, CDCl₃, 25 °C): δ = 7.03 (s, 6H; aryl CH), 474 3.68 (t, 6H; CH₂), 2.98 (t, 6H; CH₂), 2.38 (s, 9H; CH₃), 2.13 (s, 475 18H; CH₃). ¹³C NMR (126 MHz, CDCl₃, 25 °C): δ = 147.0 (ipso 476 C), 133.2 (m-CH), 119.9 (o-CMe), 119.1 (p-CMe), 59.6 (CH₂), 53.1 477 (CH_2) , 23.3 (o- CH_3), 21.4 (p- CH_3). The signal-to-noise ratio was too 478 low to properly identify any C_6F_5 ^{13}C resonances. ^{51}V NMR (105 479 MHz, CDCl₃, 25 °C): $\delta = -300.7$ (br). ¹³B NMR (128 MHz, CDCl₃, 480 25 °C): $\delta = -2.3$ (br). ³¹P NMR (161 MHz, CDCl₃, 25 °C): $\delta = 481$ 70.92 (s). ¹⁹F NMR (376 MHz, CDCl₃, 25 °C): $\delta = -134.2$ (br, 4F; 482 B o-C₆F₅), -148.0 (br, 6F; tren o-C₆F₅), -155.8 (d, 2F; quinone CF), 483 -156.6 (d, 2F; quinone CF), -160.8 (t, 2F; B p-C₆F₅), -166.9 (t, 4F; 484 B m-C₆F₅), -168.1 (d, 6F; tren o-C₆F₅), -168.7 (t, 3F; tren p-C₆F₅). 485 Elemental analysis (%) calc. for $C_{69}H_{45}BF_{29}N_5PV$ (1619.8310 g· 486 mol⁻¹): C, 51.16; H, 2.80; N, 4.32. Found: C, 50.83; H, 2.45; N, 3.96. 487

Synthesis of 2-H₄. The synthesis of **2-H₄** was carried out in a 488 manner identical to that of **2-F₄**, except benzoquinone was used in 489 place of tetrafluoro-1,4-benzoquinone. The resulting product was 490 characterized crystallographically. Single crystals suitable for XRD 491 studies were grown by the slow vapor diffusion of iso-octane into an 492 ether solution of the product.

Synthesis of $[(\hat{Ph}_2N)_3V(\mu-N)B(C_6F_5)_2][Co(C_5Me_5)_2]$ (3a). A 494 solution of $Co(C_5Me_5)_2$ (0.033 g, 0.1 mmol) in THF (2 mL) was 495 added to a solution of complex 1a (0.091 g, 0.1 mmol) in THF (3 496 mL). The reaction mixture stood at room temperature for 15 min, 497 and the solvent was removed in vacuo. The residue was washed with 498 cold ether (2 × 3 mL) to afford a brown solid (0.086 g, 0.0687 mmol, 499 68.7% yield). Single crystals suitable for XRD studies were obtained 500 by the slow vapor diffusion of pentane into a concentrated 501 difluorobenzene solution of 3a at room temperature. EPR data were 502 collected at 298 K in benzene (Figure S64) and at 100 K in THF 503 (Figure S65). Elemental analysis (%) calc. for $C_{68}H_{60}BCoF_{10}N_4V$ 504 (1243.9247 g·mol⁻¹): C, 65.66; H, 4.86; N, 4.50. Found: C, 64.62; H, 505 4.76; N, 4.21.

Synthesis of [N(Ch₂CH₂N(C₆F₅))₃V(μ -N)B(C₆F₅)₂][Co(C₅Me₅)₂] 507 (**3b**). To a stirring solution of **1b** (0.100 g, 0.0951 mmol) in ether (3 508 mL) was added Co(C₅Me₅)₂ (0.031 g, 0.0951 mmol) in ether (2 mL) 509 to immediately give a dark-red precipitate that was stirred for 15 min. 510 The volatiles were removed in vacuo, and the red powder was washed 511 with pentane (5 × 1 mL) and ether (5 × 1 mL). The brick-red 512 powder was then dried in vacuo (0.105 g, 0.0760 mmol, 79.9% yield). 513 Single crystals suitable for XRD studies were grown by the slow 514 evaporation of a 10:1 ether/DCM mixture of the product. EPR data 515 were collected at 100 K in DCM (Figure S66). Elemental analysis (%) 516 calc. for C₅₆H₄₂BCoF₂₅N₅V (1380.6318 g·mol⁻¹): C, 48.72; H, 3.07; 517 N, 5.07. Found: C, 48.99; H, 2.73; N, 4.91.

Synthesis of $[N(CH_2CH_2N(C_6F_5))_3V(\mu-N)B(C_6F_5)_2][Co(C_5H_5)_2]$ 519 (3b'). To a stirring solution of 1b (0.160 g, 0.152 mmol) in ether (4 520 mL) was added $Co(C_5H_5)_2$ (0.029 g, 0.152 mmol) in ether (2 mL) to 521 immediately give a dark precipitate that was stirred for 30 min. The 522 volatiles were removed in vacuo, and the dark residue was washed 523 with pentane (10 × 1 mL) and ether (5 × 1 mL) until the filtrate 524 wash was nearly colorless. After the removal of the remaining wash 525 solvent, a dark-red powder was isolated (0.137 g, 0.110 mmol, 72.7% 526 yield). Single crystals suitable for XRD studies were grown by the slow 527 vapor diffusion of HMDSO into a saturated DCM solution of the 528 product. EPR data were collected at 100 K in DCM (Figure S67). 529 Elemental analysis (%) calc. for $C_{46}H_{22}BCoF_{25}N_3V$ (1240.3618 g· 530 mol⁻¹): C, 44.54; H, 1.79; N, 5.65. Found: C, 44.36; H, 1.50; N, 5.59. 531

Synthesis of 4a. Method 1. A solution of 1a (0.091 g, 0.1 mmol) six in fluorobenzene (3 mL) was combined with a solution of $CO(C_5Me_5)_2$ (0.033 g, 0.1 mmol) in fluorobenzene (1 mL), and the mixture stood at room temperature overnight. The volatiles were removed in vacuo to give a dark-brown powder, and the 1H , 1P_5F , and 1P_5F (see Method 2) as the major product (>85%) (Figure SS5). Because six of the similar solubility of 4a and the minor impurities, multiple stool attempts to purify it failed.

Method 2. A solution of 3a (0.240 g, 0.193 mmol) in THF (6 mL) 541 s42 was combined with a solution of 2,4,6- ${}^{t}Bu_{3}C_{6}H_{2}O$ · (0.0505 g, 0.193 543 mmol) in THF (2 mL), and the mixture stood at room temperature 544 for 2 h. The volatiles were then removed in vacuo to give a dark-545 brown solid powder, and the ¹H NMR of this crude product revealed 546 a 1:1 mixture of 4a and 2,4,6-tBu₃PhOH. The crude powder was 547 washed with pentane $(3 \times 5 \text{ mL})$ and then with ether $(4 \times 4 \text{ mL})$ to give a dark-brown solid (0.050 g, 0.04 mmol, 20.7% yield). The 549 isolated yield was low due to the similar solubility of 4a and the 550 2,4,6-^tBu₃C₆H₂OH byproduct. Single crystals suitable for XRD studies 551 were obtained by the slow vapor diffusion of pentane into a 552 concentrated difluorobenzene solution of 4a at room temperature. ¹H 553 NMR (400 MHz, THF- d_8 , 25 °C): δ = 7.16 (t, ${}^3J_{\rm HH}$ = 7.9 Hz, 2H; m-554 ArH), 7.07 (d, ${}^{3}J_{HH}$ = 7.9 Hz, 2H; o-ArH), 6.90 (t, ${}^{3}J_{HH}$ = 7.6 Hz, 555 10H; m-ArH), 6.78 (d, ${}^{3}J_{HH}$ = 7.6 Hz, 10H; o-ArH), 6.73 (t, ${}^{3}J_{HH}$ = 556 7.2 Hz, 5H; p-ArH), 1.98 (s, 2H; BCH₂), 1.52 (s, 15H; C₅Me₅), 1.42 557 (s, 6H; CMe), 1.09 (s, 6H; CMe). ¹³C NMR (100 MHz, THF-d₈, 25 558 °C): δ = 155.6, 128.6, 128.2, 124.4, 124.1, 122.7, 119.7 (two sets of 559 phenyl resonances are observed and are attributed to π - π stacking 560 between one C₆H₅ group and one C₆F₅ group, as observed in the 561 solid-state XRD structure), 94.9, 93.7, 93.0, 91.9 (C), 8.4, 7.9, 7.4 (CMe). The signal-to-noise ratio was too low to properly identify any 563 C₆F₅ and BCH₂ ¹³C resonances. ⁵¹V NMR (105 MHz, THF-d₈, 25 564 °C): $\delta = -155.0$ (br). ¹³B NMR (128 MHz, THF- d_8 , 25 °C): $\delta =$ 565 –2.0 (br). ¹⁹F NMR (376 MHz, THF- d_8 , 25 °C): δ = –127.1 (m, 4F; 566 o-C₆F₅), -164.2 (t, J = 18.8 Hz, 2H; p-C₆F₅), -167.0 (m, 4F; m-567 C₆F₅). Elemental analysis (%) calc. for C₆₈H₅₉BCoF₁₀N₄V 568 (1242.9167 g·mol⁻¹): C, 65.71; H, 4.78; N, 4.51. Found: C, 65.35; 569 H, 5.10; N, 4.51.

Synthesis of 4b. To a stirring solution of 3b (0.050 g, 0.0362 570 571 mmol) in DCM (2 mL) was added 2,4,6-^tBu₃C₆H₂O· (0.0095 g, 572 0.0362 mmol) in DCM (1 mL) to induce an immediate color change 573 to yellow. The solution was stirred for 1 h before all volatiles were 574 removed in vacuo. The residue was washed with pentane ($10 \times 1 \text{ mL}$) 575 to remove the 2,4,6-tBu₃PhOH byproduct and residual 576 2,4,6-tBu₃PhO·. The remaining solid was then washed with ether (1 577 mL), and the remaining yellow powder was dried in vacuo (0.031 g, 578 0.0224 mmol, 62% yield). Single crystals suitable for XRD studies 579 were grown by the slow vapor diffusion of iso-octane into a 1:1 580 DCM/ether mixture of the product. NMR data: ¹H NMR (400 MHz, 581 CD₂Cl₂, 25 °C): δ = 3.65 (br, 6H; CH₂), 2.88 (br, 6H; CH₂), 1.61 582 (br, 15H; C_5Me_5) 1.51 (br, 2H; BCH_2) 1.34 (br, 6H; CMe) 0.81 (br, 583 6H; CMe). ¹³C NMR (100 MHz, CD_2Cl_2 25 °C): δ = 120.7 584 (C₅Me₅), 93.5 (CMe), 92.8 (CMe), 92.1 (CMe), 61.0 (CH₂), 55.0 585 (CH₂), 8.4 (BCH₂), 8.1 (C₅Me₅), 8.0 (CMe), 7.8 (CMe). The signal-586 to-noise ratio was too low to properly identify any C₆F₅ ¹³C 587 resonances. ⁵¹V NMR (105 MHz, $\overline{\text{CD}_2\text{Cl}_2}$, 25 °C): $\delta = -235.7$ (br). ¹³B NMR (128 MHz, CD₂Cl₂, 25 °C): $\delta = -5.5$ (br). ¹⁹F NMR (376 589 MHz, CD_2Cl_2 , 25 °C): $\delta = -127.8$ (br, 4F; B o-C₆F₅), -148.9 (br, 590 6F; tren o-C₆F₅), -162.8 (br, 2F; B p-C₆F₅), -167.5 (br, 4F; B m-591 C_6F_5), -167.4 (br, 6F; tren m- C_6F_5), -168.6 (br, 3F; tren p- C_6F_5). 592 Elemental analysis (%) calc. for $C_{56}H_{41}BCoF_{25}N_5V$ (1379.6238 g· 593 mol⁻¹): C, 48.75; H, 3.00; N, 5.08. Found: C, 48.41; H, 3.12; N, 4.97. Synthesis of $[(Ph_2N)_3V(\mu-N)B(O(O)CPh)(C_6F_5)_2][Co(C_5Me_5)_2]$ 595 (5a). The radical anion 3a was generated in situ and then reacted with 596 dibenzoyl peroxide. A solution of 1a (0.091 g, 0.1 mmol) in THF (3 597 mL) was mixed with a solution of $Co(C_5Me_5)_2$ (0.033 g, 0.1 mmol) 598 in THF (1 mL), and the solution stood at ambient temperature for 5 599 min. Dibenzoyl peroxide (12.1 mg, 0.05 mmol) in THF (1 mL) was 600 added to the above solution, and the resulting mixture stood at 601 ambient temperature for 3 h. The volatiles were removed in vacuo to

give a greasy red mixture, which was washed with ether $(3 \times 5 \text{ mL})$ to 602 give a red powder (0.075 g, 0.055 mmol, 55% yield).). Single crystals 603 suitable for XRD studies were obtained by the slow vapor diffusion of 604 pentane into a concentrated difluorobenzene solution of 4a at room 605 temperature. ¹H NMR (400 MHz, THF- d_8 , 25 °C): δ = 7.71 (d, ${}^3J_{HH}$ 606 = 7.2 Hz, 2H; o-ArH of PhCOO), 7.27 (t, ${}^{3}J_{HH}$ = 7.2 Hz, 1H; p-ArH 607 of PhCOO), 7.71 (d, ${}^{3}J_{HH}$ = 7.2 Hz, 2H; m-ArH of PhCOO), 6.80 (d, 608 $^{3}J_{HH} = 7.2 \text{ Hz}$, 12H; m-ArH of Ph₂N), 6.71 (d, $^{3}J_{HH} = 7.2 \text{ Hz}$, 12H; o- 609 ArH of Ph₂N), 6.63 (t, ${}^{3}J_{HH}$ = 7.2 Hz, 6H; p-ArH of Ph₂N), 1.70 (s, 610 30H; C_5Me_5). ¹³C NMR (100 MHz, THF- d_8 , 25 °C): δ = 166.9 611 (PhCOO), 155.4 (Ph₂N), 136.4 (PhCOO), 131.0 (PhCOO), 130.6 612 (PhCOO), 128.4 (Ph₂N), 127.7 (PhCOO), 124.7 (Ph₂N), 122.7 613 (Ph_2N) , 95.0 (C_5Me_5) , 7.9 (C_5Me_5) . The signal-to-noise ratio was too 614 low to properly identify any C_6F_5 ^{13}C resonances. ^{51}V NMR (105 615 MHz, THF- d_8 , 25 °C): $\delta = -166.4$ (br). ¹³B NMR (128 MHz, THF- 616 d_{8} , 25 °C): $\delta = -1.3$ (s). ¹⁹F NMR (376 MHz, THF- d_{8} , 25 °C): $\delta = 617$ -132.5 (m, 4F; o-C₆F₅), -164.8 (t, J = 18.8 Hz, 2F; p-C₆F₅), -168.3 618 (m, 4F; m-C₆F₅). Elemental analysis (%) calc. for 619 $C_{75}H_{65}BCoF_{10}N_4O_2V$ (1365.0397 g·mol⁻¹): C, 65.99; H, 4.80; N, 620 4.10. Found: C, 65.43; H, 4.68; N, 3.79.

Synthesis of $[N(CH_2CH_2N(C_6F_5))_3V(\mu-N)B(O(O)CPh)(C_6F_5)_2]$ - 622 $[Co(C_5H_5)_2]$ (5b'). To a stirring solution of 3b' (0.040 g, 0.0322 623 mmol) in DCM (2 mL) was added dibenzoyl peroxide (0.004 g, 624 0.016 mmol) in DCM (1 mL) to give an immediate lightening of the 625 solution to orange. The mixture was stirred for 15 min; then, all 626 volatiles were removed in vacuo. The resulting yellow-orange powder 627 was washed with pentane $(3 \times 1 \text{ mL})$ and ether $(5 \times 0.5 \text{ mL})$, and the 628 volatiles were removed in vacuo (0.032 g, 0.0235 mmol, 73% yield). 629 Single crystals suitable for XRD studies were grown by the slow vapor 630 diffusion of iso-octane into a saturated solution of the product in 631 DCM. NMR data: ¹H NMR (400 MHz, CD₂Cl₂, 25 °C): δ = 7.96 (d, 632 $^{3}J_{HH}$ = 8 Hz, 2H; o-ArH of PhCOO), 7.50 (br, 1H; p-ArH of 633 PhCOO), 7.45 (t, ${}^{3}J_{HH}$ = 8 Hz, 2H; m-ArH of PhCOO) 5.44 (s, 10H; 634 CH) 3.69 (br, 6H; CH₂) 3.00 (br, 6H; CH₂). ¹³C NMR (100 MHz, 635 CD_2Cl_2 , 25 °C): δ = 167.7 (PhCOO), 131.4 (PhCOO), 130.1 636 (PhCOO), 128.2 (PhCOO), 85.1 (C₅H₅), 60.2 (CH₂), 53.7 (CH₂). 637 The signal-to-noise ratio was too low to properly identify any C₆F₅ 638 ¹³C resonances. ⁵¹V NMR (105 MHz, CD_2Cl_2 , 25 °C): $\delta = -310.7$ 639 (br). ¹³B NMR (128 MHz, CD_2Cl_2 , 25 °C): $\delta = -4.2$ (br). ¹⁹F NMR 640 (376 MHz, CD₂Cl₂, 25 °C): $\delta = -134.0$ (br. 4F; B o-C₆F₅), -148.8 641 (br, 6F; tren o-C₆F₅), -162.6 (br, 2F; B p-C₆F₅), -168.0 (br, 4F; B 642 $m-C_6F_5$), -168.0 (br, 6F; tren $m-C_6F_5$), -169.0 (br, 3F; tren $p-C_6F_5$). 643 Elemental analysis (%) calc. for C₅₃H₂₇BCoF₂₅N₅O₂V (1361.4768 g· 644 mol⁻¹): C, 46.76; H, 2.00; N, 5.14. Found: C, 46.57; H, 1.93; N, 4.99. 645

Synthesis of (C₆H₅)₂NB(C₆F₅)₂. Diphenylamine (0.0338 g, 0.2 646 mmol) in toluene (3 mL) was added to a solution of B(C₆F₅)₃ (0.102 647 g, 0.2 mmol) in toluene (3 mL) to give a pale-yellow solution that was 648 stirred overnight at 110 °C to give a colorless solution. The volatiles 649 (including the C₆F₅H byproduct) were removed in vacuo to give a 650 pale-yellow solid, which was recrystallized in pentane at -35 °C to 651 give a white solid (0.047 g, 0.092 mmol, 46% yield). ¹H NMR (400 652 MHz, C₆D₆, 25 °C): δ = 6.95 (d, ³J_{HH} = 7.6 Hz, 4H; *o*-ArH), 6.80 (t, 653 ³J_{HH} = 7.2 Hz, 4H; *m*-ArH), 6.74 (t, ³J_{HH} = 6.8 Hz, 2H; *p*-ArH). ¹³C 654 NMR (100 MHz, C₆D₆, 25 °C): δ = 146.9 (ipso C), 129.3 (*o*-CH), 655 127.4 (*m*-CH), 126.7 (*p*-CH). The signal-to-noise ratio was too low 656 to properly identify any C₆F₅ ¹³C resonances. ¹³B NMR (128 MHz, 657 C₆D₆, 25 °C): δ = 36.7 (br). ¹⁹F NMR (376 MHz, C₆D₆, 25 °C): δ = 658 -132.4 (m, 4F; *o*-C₆F₅), -151.2 (t, *J* = 18.8 Hz, 2F; *p*-C₆F₅), -161.5 659 (m, 4F; *m*-C₆F₅). Elemental analysis (%) calc. for C₂₄H₁₀BF₁₀N 660 (513.1450 g·mol⁻¹): C, 56.18; H, 1.96; N, 2.73. Found: C, 55.92; H, 661 1.80; N, 2.62.

ASSOCIATED CONTENT

Supporting Information

The Supporting Information is available free of charge at 665 https://pubs.acs.org/doi/10.1021/acs.inorgchem.0c01464.

NMR, EPR, XRD, CV, DFT, crystallographic CIF files 667 (PDF) 668

663

664

669 Accession Codes

670 CCDC 1988821–1988833 contain the supplementary crys-671 tallographic data for this paper. These data can be obtained 672 free of charge via www.ccdc.cam.ac.uk/data_request/cif, or by 673 emailing data_request@ccdc.cam.ac.uk, or by contacting The 674 Cambridge Crystallographic Data Centre, 12 Union Road, 675 Cambridge CB2 1EZ, UK; fax: +44 1223 336033.

676 AUTHOR INFORMATION

677 Corresponding Author

Gabriel Ménard — Department of Chemistry and Biochemistry,
University of California, Santa Barbara, California 93106,
United States; orcid.org/0000-0002-2801-0863;
Email: menard@chem.ucsb.edu

682 Authors

691

692

693

694

695

Anthony Wong – Department of Chemistry and Biochemistry, University of California, Santa Barbara, California 93106, United States; orcid.org/0000-0001-6918-2437

Jiaxiang Chu – Department of Chemistry and Biochemistry,
 University of California, Santa Barbara, California 93106,
 United States; School of Chemical Science, University of Chinese
 Academy of Sciences, Beijing 101408, China
 Guang Wu – Department of Chemistry and Biochemistry.

Guang Wu – Department of Chemistry and Biochemistry, University of California, Santa Barbara, California 93106, United States

Joshua Telser – Department of Biological, Chemical, and Physical Sciences, Roosevelt University, Chicago, Illinois 60605, United States; o orcid.org/0000-0003-3307-2556

Roman Dobrovetsky – School of Chemistry, Raymond and
Beverly Sackler Faculty of Exact Sciences, Tel Aviv University,
Tel Aviv 69978, Israel

699 Complete contact information is available at: 700 https://pubs.acs.org/10.1021/acs.inorgchem.0c01464

701 Author Contributions

 $_{702}$ $^{\perp}$ A.W. and J.C. contributed equally.

703 Notes

704 The authors declare no competing financial interest.

705 **ACKNOWLEDGMENTS**

706 We thank the National Science Foundation (CHE-1900651), 707 the U.S.-Israel Binational Science Foundation (no. 2018221), 708 the ACS Petroleum Research Fund (no. 58693-DNI3), and the 709 University of California, Santa Barbara for financial support.

10 REFERENCES

- 711 (1) Frey, G. D.; Lavallo, V.; Donnadieu, B.; Schoeller, W. W.; 712 Bertrand, G. Facile Splitting of Hydrogen and Ammonia by 713 Nucleophilic Activation at a Single Carbon Center. *Science* **2007**, 714 316, 439–441.
- 715 (2) Welch, G. C.; Juan, R. R. S.; Masuda, J. D.; Stephan, D. W. 716 Reversible, metal-free hydrogen activation. *Science* **2006**, *314*, 1124–717 1126.
- 718 (3) Power, P. P. Main-group elements as transition metals. *Nature* 719 **2010**, 463, 171–177.
- 720 (4) Légaré, M.-A.; Bélanger-Chabot, G.; Dewhurst, R. D.; Welz, E.; 721 Krummenacher, I.; Engels, B.; Braunschweig, H. Nitrogen fixation and 722 reduction at boron. *Science* **2018**, *359*, 896–900.
- 723 (5) Hicks, J.; Vasko, P.; Goicoechea, J. M.; Aldridge, S. Synthesis, 724 structure and reaction chemistry of a nucleophilic aluminyl anion. 725 *Nature* **2018**, 557, 92–95.
- 726 (6) Stephan, D. W. The broadening reach of frustrated Lewis pair 727 chemistry. *Science* **2016**, 354, 1248.

- (7) Stephan, D. W.; Erker, G. Frustrated Lewis Pair Chemistry: 728 Development and Perspectives. *Angew. Chem., Int. Ed.* **2015**, *54*, 729 6400–6441.
- (8) Stephan, D. W. Frustrated Lewis Pairs: From Concept to 731 Catalysis. Acc. Chem. Res. 2015, 48, 306–316.
- (9) Grimme, S.; Kruse, H.; Goerigk, L.; Erker, G. The Mechanism of 733 Dihydrogen Activation by Frustrated Lewis Pairs Revisited. *Angew.* 734 *Chem., Int. Ed.* **2010**, *49*, 1402–1405.
- (10) Rokob, T. A.; Hamza, A.; Stirling, A.; Soós, T.; Pápai, I. 736 Turning Frustration into Bond Activation: A Theoretical Mechanistic 737 Study on Heterolytic Hydrogen Splitting by Frustrated Lewis Pairs. 738 Angew. Chem., Int. Ed. 2008, 47, 2435–2438.
- (11) Bannwarth, C.; Hansen, A.; Grimme, S. The Association of 740 Two "Frustrated" Lewis Pairs by State-of-the-Art Quantum Chemical 741 Methods. *Isr. J. Chem.* **2015**, *55*, 235–242.
- (12) Liu, L.; Cao, L. L.; Shao, Y.; Ménard, G.; Stephan, D. W. A 743 Radical Mechanism for Frustrated Lewis Pair Reactivity. *Chem.* **2017**, 744 3, 259–267.
- (13) Merk, A.; Großekappenberg, H.; Schmidtmann, M.; Luecke, 746 M.-P.; Lorent, C.; Driess, M.; Oestreich, M.; Klare, H. F. T.; Müller, 747 T. Single-Electron Transfer Reactions in Frustrated and Conventional 748 Silylium Ion/Phosphane Lewis Pairs. *Angew. Chem., Int. Ed.* **2018**, 57, 749 15267—15271.
- (14) Liu, L. L.; Cao, L. L.; Zhu, D.; Zhou, J.; Stephan, D. W. 751 Homolytic cleavage of peroxide bonds via a single electron transfer of 752 a frustrated Lewis pair. *Chem. Commun.* **2018**, *54*, 7431–7434.
- (15) Dong, Z.; Cramer, H. H.; Schmidtmann, M.; Paul, L. A.; 754 Siewert, I.; Müller, T. Evidence for a Single Electron Shift in a Lewis 755 Acid–Base Reaction. *J. Am. Chem. Soc.* **2018**, *140*, 15419–15424.
- (16) Liu, L. L.; Stephan, D. W. Radicals derived from Lewis acid/ 757 base pairs. *Chem. Soc. Rev.* **2019**, *48*, 3454–3463.
- (17) Piers, W. E.; Marwitz, A. J. V.; Mercier, L. G. Mechanistic 759 Aspects of Bond Activation with Perfluoroarylboranes. *Inorg. Chem.* 760 **2011**, 50 (24), 12252–12262.
- (18) Soltani, Y.; Dasgupta, A.; Gazis, T. A.; Ould, D. M. C.; 762 Richards, E.; Slater, B.; Stefkova, K.; Vladimirov, V. Y.; Wilkins, L. C.; 763 Willcox, D.; Melen, R. L. Radical Reactivity of Frustrated Lewis Pairs 764 with Diaryl Esters. *Cell Rep. Phys. Sci.* **2020**, *1*, 100016.
- (19) Braunschweig, H.; Dyakonov, V.; Jimenez-Halla, J. O. C.; Kraft, 766 K.; Krummenacher, I.; Radacki, K.; Sperlich, A.; Wahler, J. An Isolable 767 Radical Anion Based on the Borole Framework. *Angew. Chem., Int. Ed.* 768 **2012**, 51, 2977–2980.
- (20) Bauer, J.; Braunschweig, H.; Hörl, C.; Radacki, K.; Wahler, J. 770 Synthesis of Zwitterionic Cobaltocenium Borate and Borata-alkene 771 Derivatives from a Borole-Radical Anion. *Chem. Eur. J.* **2013**, *19*, 772 13396–13401.
- (21) Silva Valverde, M. F.; Schweyen, P.; Gisinger, D.; Bannenberg, 774 T.; Freytag, M.; Kleeberg, C.; Tamm, M. N-Heterocyclic Carbene 775 Stabilized Boryl Radicals. *Angew. Chem., Int. Ed.* **2017**, *56*, 1135–776 1140.
- (22) Cao, L. L.; Stephan, D. W. Homolytic Cleavage Reactions of a 778 Neutral Doubly Base Stabilized Diborane(4). *Organometallics* **2017**, 779 36, 3163–3170.
- (23) Su, Y.; Kinjo, R. Boron-containing radical species. *Coord. Chem.* 781 *Rev.* **2017**, 352, 346–378.
- (24) Wong, A.; Guevara, K.; Wu, G.; Ménard, G. Unusual C-H 783 Bond Activation and C(sp3)-C(sp3) Bond Formation at an Fe(II) 784 Bis(amide) Carbene Complex. *Organometallics* **2020**, 39, 116–122. 785
- (25) Carroll, T. G.; Hunt, C.; Garwick, R.; Wu, G.; Dobrovetsky, R.; 786 Ménard, G. An untethered C3v-symmetric triarylphosphine oxide 787 locked by intermolecular hydrogen bonding. *Chem. Commun.* **2019**, 788 55, 3761–3764.
- (26) Carroll, T. G.; Garwick, R.; Telser, J.; Wu, G.; Ménard, G. 790 Synthesis, Characterization, and Electrochemical Analyses of 791 Vanadocene Tetrametaphosphate and Phosphinate Derivatives. 792 Organometallics 2018, 37, 848–854.
- (27) Carroll, T. G.; Garwick, R.; Wu, G.; Ménard, G. A Mono-, Di-, 794 and Trivanadocene Phosphorus Oxide Series: Synthesis, Magnetism, 795

- 796 and Chemical/Electrochemical Properties. *Inorg. Chem.* **2018**, *57*, 797 11543–11551.
- 798 (28) Chu, J.; Carroll, T. G.; Wu, G.; Telser, J.; Dobrovetsky, R.; 799 Ménard, G. Probing Hydrogen Atom Transfer at a Phosphorus(V) 800 Oxide Bond Using a "Bulky Hydrogen Atom" Surrogate: Analogies to 801 PCET. J. Am. Chem. Soc. 2018, 140, 15375–15383.
- 802 (29) Parks, D. J.; Piers, W. E.; Yap, G. P. A. Synthesis, Properties, 803 and Hydroboration Activity of the Highly Electrophilic Borane 804 Bis(pentafluorophenyl)borane, HB(C6F5)2. *Organometallics* 1998, 805 17, 5492–5503.
- 806 (30) Song, J.-I.; Gambarotta, S. Preparation, Characterization, and 807 Reactivity of a Diamagnetic Vanadium Nitride. *Chem. Eur. J.* **1996**, 2, 808 1258–1263.
- 809 (31) Kol, M.; Schrock, R. R.; Kempe, R.; Davis, W. M. Synthesis of 810 Molybdenum and Tungsten Complexes That Contain Triamidoamine 811 Ligands of the Type (C6F5NCH2CH2)3N and Activation of 812 Dinitrogen by Molybdenum. *J. Am. Chem. Soc.* **1994**, *116*, 4382—813 4390.
- 814 (32) Wagner, C. L.; Phan, N. A.; Fettinger, J. C.; Berben, L. A.; 815 Power, P. P. New Characterization of V{N(SiMe3)2}3: Reductions of 816 Tris[bis(trimethylsilyl)amido]vanadium(III) and -chromium(III) To 817 Afford the Reduced Metal(II) Anions [M{N(SiMe3)2}3] (M = V 818 and Cr). *Inorg. Chem.* **2019**, *58*, 6095–6101.
- 819 (33) Galsworthy, J. R.; Green, M. L. H.; Clifford Williams, V.; 820 Chernega, A. N. Syntheses and characterization of amino-821 (pentafluorophenyl)boranes. Crystal structure of [(Me3Si)2NB-822 (C6FS)2]. *Polyhedron* 1998, 17, 119–124.
- (34) Bamford, K. L.; Longobardi, L. E.; Liu, L.; Grimme, S.; 824 Stephan, D. W. FLP reduction and hydroboration of phenanthrene o-825 iminoquinones and α -diimines. Dalton Trans. 2017, 46, 5308-5319. (35) Yi, J.; Yang, W.; Sun, W.-H.; Nomura, K.; Hada, M. Vanadium 826 827 NMR Chemical Shifts of (Imido)vanadium(V) Dichloride Complexes 828 with Imidazolin-2-iminato and Imidazolidin-2-iminato Ligands: 829 Cooperation with Quantum-Chemical Calculations and Multiple 830 Linear Regression Analyses. J. Phys. Chem. A 2017, 121, 9099-9105. (36) Danopoulos, A. A.; Redshaw, C.; Vaniche, A.; Wilkinson, G.; 832 Hussain-Bates, B.; Hursthouse, M. B. Organoimido complexes of tungsten. X-ray crystal structures of W(NC6H11)Cl2(PMe3)3, [W(NC6H11)Cl2(PMe3)3]O3SCF3, [W(NC6H11)Cl(PMe3)4]-835 BPh4, W[NSi(o-MeC6H4)3]Cl2(PMe3)3, W[NB(mes2)]2Cl2-836 (PMe3)2, {W(NPh)Cl[O2C2(CF3)4]2}Li and WCl4(PMe2Ph)3. 837 Polyhedron 1993, 12, 1061-1071.
- 838 (37) Weber, K.; Korn, K.; Schorm, A.; Kipke, J.; Lemke, M.; 839 Khvorost, A.; Harms, K.; Sundermeyer, J. Recent Advances in the 840 Synthesis of N-Heteroatom Substituted Imido Complexes Containing 841 a Nitrido Bridge [M = N—E] (M = Group 4, 5 and 6 Metal, E = B, 842 Si, Ge, P, S). Z. Anorg. Allg. Chem. 2003, 629, 744–754.
- 843 (38) Thompson, R.; Chen, C.-H.; Pink, M.; Wu, G.; Mindiola, D. J. 844 A Nitrido Salt Reagent of Titanium. *J. Am. Chem. Soc.* **2014**, *136*, 845 8197–8200.
- 846 (39) Stevenson, L. C.; Mellino, S.; Clot, E.; Mountford, P. Reactions 847 of Titanium Hydrazides with Silanes and Boranes: N–N Bond 848 Cleavage and N Atom Functionalization. *J. Am. Chem. Soc.* **2015**, *137*, 849 10140–10143.
- 850 (40) Clough, B. A.; Mellino, S.; Clot, E.; Mountford, P. New 851 Scandium Borylimido Chemistry: Synthesis, Bonding, and Reactivity. 852 *J. Am. Chem. Soc.* **2017**, *139*, 11165–11183.
- 853 (41) Clough, B. A.; Mellino, S.; Protchenko, A. V.; Slusarczyk, M.; 854 Stevenson, L. C.; Blake, M. P.; Xie, B.; Clot, E.; Mountford, P. New 855 Titanium Borylimido Compounds: Synthesis, Structure, and Bonding. 856 *Inorg. Chem.* **2017**, *56*, 10794–10814.
- 857 (42) Espada, M. F.; Bennaamane, S.; Liao, Q.; Saffon-Merceron, N.; 858 Massou, S.; Clot, E.; Nebra, N.; Fustier-Boutignon, M.; Mézailles, N. 859 Room-Temperature Functionalization of N2 to Borylamine at a 860 Molybdenum Complex. *Angew. Chem., Int. Ed.* 2018, 57, 12865—861 12868.
- 862 (43) Piers, W. E. The Chemistry of Perfluoroaryl Boranes. In 863 Advances in Organometallic Chemistry; Academic Press: 2005; Vol. 52, 864 pp 1-76.

- (44) Ménard, G.; Hatnean, J. A.; Cowley, H. J.; Lough, A. J.; 865 Rawson, J. M.; Stephan, D. W. C-H Bond Activation by Radical Ion 866 Pairs Derived from R3P/Al(C6F5)3 Frustrated Lewis Pairs and N2O. 867 *J. Am. Chem. Soc.* **2013**, 135, 6446–6449.
- (45) Culcasi, M.; Berchadsky, Y.; Gronchi, G.; Tordo, P. Anodic 869 behavior of crowded triarylphosphines. ESR study of triarylphospho-870 niumyl radicals, Ar3P(*+). *J. Org. Chem.* **1991**, 56, 3537–3542. 871
- (46) Connelly, N. G.; Geiger, W. E. Chemical Redox Agents for 872 Organometallic Chemistry. *Chem. Rev.* **1996**, 96, 877–910.
- (47) Agarwal, P.; Piro, N. A.; Meyer, K.; Müller, P.; Cummins, C. C. 874 An Isolable and Monomeric Phosphorus Radical That Is Resonance-875 Stabilized by the Vanadium(IV/V) Redox Couple. *Angew. Chem., Int.* 876 Ed. 2007, 46, 3111–3114.
- (48) Cutsail, G. E., III; Stein, B. W.; Subedi, D.; Smith, J. M.; Kirk, 878 M. L.; Hoffman, B. M. EPR, ENDOR, and Electronic Structure 879 Studies of the Jahn—Teller Distortion in an FeV Nitride. *J. Am. Chem.* 880 Soc. 2014, 136, 12323—12336.
- (49) Wang, L.; Li, J.; Zhang, L.; Fang, Y.; Chen, C.; Zhao, Y.; Song, 882 Y.; Deng, L.; Tan, G.; Wang, X.; Power, P. P. Isolable Borane-Based 883 Diradical and Triradical Fused by a Diamagnetic Transition Metal 884 Ion. J. Am. Chem. Soc. 2017, 139, 17723–17726.
- (50) As described in ref 48, electron-nuclear double resonance 886 (ENDOR) spectroscopy has shown hyperfine coupling to 11 B (I = 3/887 2, 80%) in an S = 1/2 Fe^V complex supported by a tris(imidazolyl) 888 phenylborate ligand. However, the coupling was very weak (maximum 889 magnitude ~1.5 MHz), much too small to affect the EPR spectra. 890 Therefore, EPR spectroscopy may not be sensitive enough to detect 891 significant hyperfine coupling to 11 B in compounds 3a and 3b/3b'. 892 (51) The spin Hamiltonian parameters obtained from the EPR 803
- (51) The spin Hamiltonian parameters obtained from the EPR 893 spectrum of **3b**, namely, the g values and ⁵¹V hyperfine coupling 894 constants, were reproduced by DFT calculations. These calculations 895 suggested rhombicity in both g and $A(^{51}V)$ that was not resolvable by 896 X-band EPR spectroscopy. Therefore, for the ease of comparison, we 897 converted the calculated rhombic tensors (see the SI) to axial ones by 898 taking the average of the two closest components. This gives: 899 calculated g = [1.971, 1.971, 1.985] ($g_{\rm iso} = 1.976$); $A(^{51}V) = [-100, 900 -100, -280]$ MHz ($a_{\rm iso} = -160$ MHz), to be compared with 901 experimental: g = [1.980, 1.980, 1.962] ($g_{\rm iso} = 1.974$); $|A(^{51}V)| = [80, 902 80, 315]$ MHz ($|a_{\rm iso}| = 160$ MHz).
- (52) Buchholz, D.; Astruc, D. The First Decaisopropylmetallocene: 904 One-Pot Synthesis of [Rh(C5iPrS)2]PF6 from [Rh(C5MeS)2]PF6 905 by Formation of 20 Carbon—Carbon Bonds. *Angew. Chem., Int. Ed.* 906 *Engl.* **1994**, 33, 1637—1639.
- (53) Buchholz, D.; Gloaguen, B.; Fillaut, J.-L.; Cotrait, M.; Astruc, 908 D. Mono- and Bis(pentaisopropylcyclopentadienyl) Cobalt and 909 Rhodium Sandwich Complexes and Other Decabranched Cyclo- 910 pentadienyl Complexes. *Chem. Eur. J.* **1995**, *1*, 374–381.
- (54) Hartmann, N. J.; Wu, G.; Hayton, T. W. Trapping of an NiII 912 Sulfide by a CoI Fulvene Complex. *Organometallics* **2017**, 36, 1765–913 1769.
- (55) Preut, H.; Haupt, H.-J.; Huber, F. Die Kristall-und 915 Molekularstruktur des Hexaphenyl-distannans. Z. Anorg. Allg. Chem. 916 1973, 396, 81–89.
- (56) Manner, V. W.; Markle, T. F.; Freudenthal, J. H.; Roth, J. P.; 918 Mayer, J. M. The first crystal structure of a monomeric phenoxyl 919 radical: 2,4,6-tri-tert-butylphenoxyl radical. *Chem. Commun.* **2008**, 920 256–258.
- (57) Belford, R. L.; Belford, G. G. Eigenfield expansion technique for 922 efficient computation of field-swept fixed-frequency spectra from 923 relaxation master equations. *J. Chem. Phys.* **1973**, *59*, 853–854.
- (58) Neese, F. Software update: the ORCA program system, version 925 4.0. WIREs Comput. Mol. Sci. 2018, 8, e1327.
- (59) Grimme, S. Accurate Calculation of the Heats of Formation for 927 Large Main Group Compounds with Spin-Component Scaled 928 MP2Methods. *J. Phys. Chem. A* **2005**, *109*, 3067–3077.
- (60) Quintal, M. M.; Karton, A.; Iron, M. A.; Boese, A. D.; Martin, J. 930 M. L. Benchmark Study of DFT Functionals for Late-Transition- 931 Metal Reactions. *J. Phys. Chem. A* **2006**, *110*, 709–716.

- 933 (61) Weigend, F.; Ahlrichs, R. Balanced basis sets of split valence, 934 triple zeta valence and quadruple zeta valence quality for H to Rn: 935 Design and assessment of accuracy. *Phys. Chem. Chem. Phys.* **2005**, 7, 936 3297–3305.
- 937 (62) Lenthe, E. v.; Baerends, E. J.; Snijders, J. G. Relativistic regular 938 two-component Hamiltonians. *J. Chem. Phys.* **1993**, 99, 4597–4610. 939 (63) Lenthe, E. v.; Baerends, E. J.; Snijders, J. G. Relativistic total 940 energy using regular approximations. *J. Chem. Phys.* **1994**, *101*, 9783– 941 9792.
- 942 (64) Wüllen, C. v. Molecular density functional calculations in the 943 regular relativistic approximation: Method, application to coinage 944 metal diatomics, hydrides, fluorides and chlorides, and comparison 945 with first-order relativistic calculations. *J. Chem. Phys.* **1998**, *109*, 946 392–399.
- 947 (65) Worrell, W. L.; Chipman, J. The Free Energies of Formation of 948 the Vanadium, Niobium, and Tantalum Carbides1. *J. Phys. Chem.* 949 **1964**, 68, 860–866.